Available on line www.jocpr.com

Journal of Chemical and Pharmaceutical Research

J. Chem. Pharm. Res., 2010, 2(5):587-598

ISSN No: 0975-7384
CODEN(USA): JCPRC5

RSK2 Binding Models Delineate Key Features for Activity

Rick Gussio *[a], Michael J. Currens [b], Dominic A. Scudiero [c], Jeffrey A. Smith [d], Deborah A. Lannigan [d], Robert H. Shoemaker [b], Dan W. Zaharevitz [a], and Tam Luong Nguyen * [e, f]

[a] *Information Technology Branch, Developmental Therapeutics Program, National Cancer Institute, Frederick, Maryland 21702 (USA)*
[b] *Screening Technologies Branch, Developmental Therapeutics Program, National Cancer Institute, Frederick, Maryland 21702 (USA)*
[c] *In Vitro Screening Laboratory, SAIC-Frederick, Inc., NCI-Frederick*
[d] *Center for Cell Signaling, and Departments of Pathology and Microbiology, University of Virginia, Charlottesville, Virginia 22908 USA*
[e] *Target Structure-based Drug Discovery Group, SAIC-Frederick, Inc., NCI-Frederick Frederick, MD 21702 (USA)*
[f] *Path Pharma, Inc., Frederick, MD 21704 (USA)*

ABSTRACT

Due to its overexpression and activation in human cancer cells and tissues, an emerging molecular target in cancer therapeutics is p90 ribosomal s6 kinase 2 (RSK2). While a growing number of RSK2 inhibitors have been reported in the literature, only the crystal structure of RSK2 in complex with an AMP analogue provides a structural basis for understanding RSK2 inhibition. To remedy this, we used our fluorescence polarization assay to determine the RSK2 activity for a set of structurally diverse compounds, and followed this by modeling their binding modes in an all-atom, energy refined crystal structure of RSK2. These binding models reveal that Val131 and Leu147 are key interaction sites for potent RSK2 inhibition. This structure-based pharmacophore is an important tool for new lead discovery and refinement.

Keywords: RSK2, binding modes, structure-based pharmacophores, cancer, kinase, inhibition, interaction sites, indirubins, flavopiridol, SL0101, BI-DI870, Ro31-8220, GF109203x, NSC 356821

INTRODUCTION

Ribosomal S6 kinase 2 (RSK2) is a serine/threonine kinase that belongs to the AGC subfamily in the human kinome. RSK2 is among four RSK isoforms that are products of separate genes with a 75%-80% sequence identity [1-4]. In the cell, RSK2 plays an important role in the MAPK signaling cascade and has attracted interest as a therapeutic target due to its link to different human diseases [5,6]. The first disease associated with RSK2 was Coffin-Lowry syndrome (CLS), which is a rare X-linked disorder that is characterized by mental retardation and dysmorphism. Mutations in the RSK2 gene were identified as the cause of CLS [7,8]. Additionally, RSK2 protein may play a role in HIV infection. RSK2 is recruited and activated by HIV-1 Tat, and is itself also important to normal Tat function [9]. Recently, RSK2 was linked to human cancers due to its overexpression in cancer cells and cancer tissues [10,11]. RSK2 is activated in head and neck squamous cell carcinoma [12]. The mechanistic basis for RSK2's role in cancer is beginning to emerge with the recent reports that RSK2 is a regulator in cell transformations induced by tumor promoters [13], and a regulator of fibroblast growth factor receptor (FGFR) [14,15].

RSK2 contains two non-identical ATP-binding sites, one located in its N-terminal kinase domain (NTKD), and a second in its C-terminal kinase domain (CTKD) [1]. While the CTKD ATP-binding site is responsible for the autophosphorylation of RSK2, which permits maximal activity of the enzyme [16], the NTKD ATP-binding site is responsible for phosphorylating exogenous substrates [17]. Due to this, the primary site for investigative small molecule inhibition of RSK2 has been at the NTKD ATP-binding site. Crystallographic analysis of the RSK family of kinases is beginning to provide important insights into their structure and function. The RSK2 CTKD has been solved to 2.00 Å and provides a structural basis for the autoactivation of RSK [18]. Recently, the crystal structures of RSK1 NTKD in complex with adenosine-5'-[β,γ-methylene]triphosphate, staurosporine, and purvalanol A have been solved [19], and, the structure of RSK2 in complex with AMP-PNP has been reported [20].

A wide array of RSK2 inhibitors has been reported in the literature, and among these, several compounds have been shown to selectively bind to the NTKD ATP-binding site [5]. Figure 1 shows a representative set of RSK2 NTKD inhibitors. The first inhibitor is kaemperfol-glycoside **1** (SL0101) [21,22], which has a IC_{50}'s of 89 nM and was shown to be specific for the RSK NTKD ATP-binding site. The second is dihydropteridinone **2** (BI-D1870) [23], which has a RSK2 IC_{50}'s of 24 nM and was also shown to be specific for the RSK NTKD ATP-binding site. There are the two classic PKC (Protein Kinase C) inhibitors, **3** (Ro31-8220) [24] and **4** (GF109203X) [25], which inactivate RSK2 with IC_{50}'s of 36 nM and 310 nM, respectively. Additionally, we previously identified benzenecarboximidamide **5** (NSC356821), a compound obtained from the National Cancer Institute chemical repository, as a potent new RSK2 inhibitor with an IC_{50} of 1 μM [26]. More recently, sizable panels of small molecule kinase inhibitors have been examined against RSK2. Bain, J et al. reported the activity of 65 well-known kinase inhibitors against RSK1 and RSK2 [27], and Bamborough et al. [28] reported the activity of 200 kinase inhibitors against RSK2. In this paper, we determined the RSK2 activity of a set of prototypical kinase inhibitors using our fluorescence polarization assay, and modeled their binding modes to delineate key interactions for ligand binding.

EXPERIMENTAL SECTION

Assay of RSK2 inhibition. Recombinant RSK2 enzyme was prepared as previously described [29]. Fluoroscein-labeled peptide substrate for RSK2 NTKD and IMAP™ beads for capturing phosphorylated product were purchased from Molecular Devices. These reagents were combined in assay buffer containing 10 μM ATP and test compound to a final volume of 20 μL. After binding to IMAP™ beads, phosphorylated substrate was detected by fluorescence polarization spectroscopy. Half-maximal inhibitory concentrations (IC_{50}) were read from concentration-response curves by linear interpolation.

Molecular modeling. Small molecule structures were built using the Biopolymer module of Insight II (Accelrys, San Diego, CA) and energy minimized in Discover using the CFF91 force-field and the VA09A algorithm with a convergence criterion of 1.0×10^{-3} kcal/mol. All simulations were performed using the CFF91 force-field with the nonbonded interaction limited to 13 Å and a distance-dependent dielectric constant using Discover 3.0 (Accelrys, San Diego, CA). The HINT program [30] (eduSoft, Richmond, VA) was used to evaluate the hydropathic quality of the interatomic interactions, and the PROCHECK program [31] was used to determine the quality of the protein model. Sequence analyses were performed using the Homology module in Insight II. PILOT is an in-house software program developed at the NCI for pharmacophoric analysis of compound set.

Initially, the inhibitors were aligned in gas-phase with ATP in a pharmacophoric fashion, using PILOT agglomerative clustering to identify common pharmacophores in the series of molecules as well as their corresponding conformational isomers. This clustering method initiates by utilizing the most rigid compound and conformers of the series as a template to prioritize triplet center type identification. Pharmacophoric centers consist of hydrogen bond acceptor, hydrogen bond donor, aromatic and hydrophobic types. All conformers of the series are iteratively clustered until all possible pharmacophore triplets are assigned to a cluster. Within a given cluster (pharmacophoric model), all molecules are aligned to the template by singular value decomposition least squares. The best pharmacophoric model is determined as having the greatest number of molecules with the lowest r.m.s. deviation for their respective pharmacophoric triplets and steric overlaps. Subsequently, this model is subjected is to a secondary pharmacophoric organization to identify additional centers beyond the initial triplet model.

The protein template for the binding models was the RSK2 NTKD crystal structure (PDB code 3G51) [20]. The individual gas-phase ligand conformations obtained from the PILOT were docked into the ATP pocket of the RSK2 NTKD model. The ligand conformations were energy minimized and scored using the HINT program [30]. The best HINT scoring poses were further refined using stepwise changes in the conformations of both the RSK2 NTKD structure and the ligands. Iterative cycles of constrained molecular dynamics simulations were employed to remove unfavorable protein-ligand interactions. During the initial minimization and dynamics simulations, the ligand conformation was fixed in Cartesian space using constraints. When the conformational changes in RSK2 reached an asymptotical point, the constraints were released from the ligand conformation. This process was iterated until the maximum HINT favorable contacts were achieved.

RESULTS

Identification of novel RSK inhibitor chemotype. We used our fluorescence polarization assay to screen small chemical libraries for RSK2 inhibition. Figure 2 shows the chemical structures and RSK2 activities of the top hits. Compounds **6-20** have activity from 0.1 µM to 3.7 µM. Indirubin-3'-oxime **6** and SB2167663 **7** are the most active compounds and both have IC_{50}'s of 1 µM. The RSK2 activities of compounds **7, 8, 11, 12, 13, 15** and **19** have previously been reported by Bain, J et al. with similar activity levels as shown here [27]. The relative activities of **6-19** reported here were used to determine their binding modes in RSK2 NTKD ATP-binding site.

Delineating a structural basis for inhibition using molecular modeling. To extend our understanding of RSK2 inhibition, binding models were constructed for compounds **1-19**. Binding models for compounds **1, 4,** and **5** in complex with RSK2 NTKD has previously been reported [26]. Examination of the binding models across the different chemotypes revealed that activity correlated with binding interactions at several key sites in RSK2 NTKD ATP-binding site. For this report, these key interactions are highlighted by contrasting the binding models of highly potent inhibitors **2** and **6** with those of weaker inhibitors **17-19**.

As shown in Figure 3, the binding model of **2** illustrates how well the compound is suited for the NTKD ATP site. The optimal packing of **2** in RSK2 may be the basis for its RSK specificity [23]. Compound **2** forms three hydrogen bonds to RSK2. One is between the hinge residues Leu150 amide NH and the 3-nitrogen of its pteridine functionality; the second is between the Leu150 backbone oxygen atoms and the secondary amine; the third is between the Thr210 side chain hydroxyl and the pteridine keto oxygen atom. These hydrogen bonding interactions are complemented by stabilizing hydrophobic interactions. At the bottom of the ATP site, the N-methyl group of **2** is wedged into a small hydrophobic pocket formed by Val131 and Leu147 and at the top of the ATP site, the dichlorophenyl ring is packed against the aromatic side chain of Phe149. Robust hydrophobic interactions are also observed between the methylisobutyl functionality of **2** and the hydrophobic isopropyl side chain of Val82 with the two moieties forming a highly favorable hydrophobic patch. Because compound **2** contains a methyl substituent at a chiral center, additional hydrophobic packing is dependent on the stereochemistry. In the R-isomer, this methyl group is packed against the hydrophobic side chain of Val82 whereas in the S-isomer, this methyl group interacts with the side chain $-CH_3$ group of Thr210, as illustrated in Figure 3 which shows the S-isomer.

The binding model of **6** shows that the molecule closely interacts with the hinge residues Asp148 and Leu150 with its indol-2-one group hydrogen bonded to the Asp148 backbone oxygen and the Leu150 backbone nitrogen (Figure 3). Additionally, the indole functionality that forms these two hydrogen bonds is wedged between the hydrophobic side chains of Val131 and Leu147. Outside of the adenine region, the oxime oxygen of **6** is hydrogen bonded to the carboxylate side chain of Asp211 via a water bridge and the indole functionality associated with this water-mediated hydrogen bond is packed against the Gly75.

Figure 4 shows the binding models of the lower affinity inhibitors **17-19**. This class of RSK2 inhibitors establishes similar hydrogen bonds as the high affinity class compounds. For **17**, the

quinoline nitrogen is hydrogen bonded to the Leu150 amide NH and its guanidine group is in a reinforced hydrogen bond with the carboxylate side chain of Asp211 (Figure 4). For **18,** its keto and 5-hydroxyl groups are hydrogen bonded to backbone atoms of Asp148 and Leu150. The piperidine-substituted hydroxyl group is hydrogen bonded to the backbone oxygen of Glu197 (Figure 4). Compound **19** is the smallest compound in the set with a molecular weight of 220. Not unexpectedly, **19** binds at the ATP site with its pyrazole motif hydrogen bonded to the hinge residues Asp148 and Leu150 (Figure 4).

Identification of critical binding interactions. Mapping the contacts between the ligands and RSK2 within specified distances is a robust method for determining crucial binding contacts. Table 1 shows the atom-atom contacts of compounds **2, 6, 17, 18**, and **19** to RSK2 that occur at 4.5 Å or less. Consistent with their activities, compounds **2** and **6** are characterized by more contacts than those evident for **17-19**. In addition to the greater number of contacts, specific interaction sites appear to be crucial. Based on the residue alignments, these crucial interaction sites belong to Val131 and Leu147. Whereas none of the three lower affinity inhibitors display contacts to Val131 and Leu147, each of the potent RSK2 inhibitors **2, 6,** and **20** are characterized by extensive contacts to hydrophobic side chains of Val131 and Leu147.

Similar to the "hot spot" concept that was used to delineate the functional epitope at protein-protein interfaces [32], Val131 and Leu147 define one of the core contacts that provide significant binding energy as evident by the RSK2 activities of compounds **2** and **6** compared with compounds **17-19**. Located in the hydrophobic interior of the ATP pocket, Val131 and Leu147 are on opposite sides of the pocket, and form a hydrophobic pocket that appears to be critical to binding affinity. The topology of Val131 and Leu147 allows inhibitors to wedge themselves onto a large hydrophobic surface. Because the adenine motif of ATP does not possess a similar wedge motif, these two "hot spots" represent important binding sites for novel small-molecule inhibitors. Because the hydrophobic effect is the central driving force behind ligand binding, identifying these two key hydrophobic interaction sites provides a structural basis for lead optimization for RSK2. The role of these two residues in binding affinity is currently being investigated and will be the subject of a later report.

DISCUSSION

Counterpart binding modes in CDK, ROCK, PKA, and c-JNK. Because of their therapeutic potential, it is not surprising that binding modes of **6-19** against other molecular targets have been extensively investigated. In fact, the X-ray structures of nine of the fourteen (compounds **6, 8, 9, 11, 12, 14, 15, 18,** and **19)** have been determined in complex with serine/threonine kinases outside of RSK2. In each instance, the RSK2 modeled binding modes are similar to those in the X-ray structures. For the hinge region, the conformations of the residues 148-154 of RSK2 are similar to the hinge segments in CDK2, ROCK2, PK, and c-JNK. This is depicted in Figure 5 which show the binding models of **8, 9, 12**, and **19** relative to their binding modes in the X-ray structures of PKA (PDB code 1YDR), CDK2 (1PF8), ROCK2 (2H9V), and c-JNK (1UKI), respectively.

Besides their RSK2 activity, compounds **6-19** inhibited kinases such as CDK, Raf1, GSK-3, ROCK, PKA, and c-JNK, which are of therapeutic interests in a variety of diseases. For

example, CDKs are key regulators that govern normal cell division, and accordingly, are attractive anticancer targets [33]. Raf1 is one of the proteins in the MEK-ERK pathway, which is associated with neuronal survival [34]. GSK-3 is an important regulatory of multiple signaling pathways and is associated with a number of different human diseases such as cancer, neurodegenerative diseases, and inflammation [35]. ROCK is involved in cell motility [36] and has therapeutic indications in hypertension [37], atherosclerosis [38] and immunosuppression [39]. c-JNK is a member of the mitogen-activated protein kinase (MAPK) group of signaling proteins and is a therapeutic target for inflammation, neurodegenerative diseases, obesity, diabetes and cancer [40]. In the phylogenetic tree of the human kinome [41], RSK2, ROCK and PKA are members of the AGC subfamily, Raf1 is a member of the TKL subfamily, and the three kinases CDK, GSK-3 and c-JNK are constituents of the CMGC subfamily. Based on the activity of **6-19**, there appears to be a strong connectivity between the AGC subfamily of RSK and the CGMC subfamily which is typified by CDK.

Crystallographic studies revealed that **6** binds at the ATP site of both CDK5 [42] (PDB code 1UNH) and GSK-3β [43] (PDB code 1Q41). Because of its efficacy against both CDK and GSK-3, compound **6** is of immense medicinal interest. Compounds **9** (SU9516) and **13** (GW5074) belong to the same indol-2-one based class as compound **6** and possess IC_{50}'s of 0.24 µM and 1.0 µM, respectively. Compound **9** (SU9516) is reported to be a CDK inhibitor [44] and its X-ray structure in complex with CDK2 has been solved (PDB code 1PF8) [45], and shows that **9** binds at the ATP site. Lastly, **13** is a Raf1 inhibitor [34,46].

As a well-known GSK-3 inhibitor [47], compound **7** (SB216763) is among the most potent RSK2 small molecule inhibitors with an IC_{50} of ~0.1 µM. The pyridine class compound **8** (Y-27632) is highly active against RSK2 with an IC_{50} of 0.21 µM and was previously of interest as a ROCK inhibitor [48]. Compound **8** exhibited a remarkable selectivity profile [49]. The crystal structure of **8** in complex with ROCK1 (PDB code 2H9V) [48] and with PKA [50] (PDB code 1Q8T) confirmed that it is ATP-competitive.

Compounds **10** (HA-100), **12** (H-7), **11** (H-8), **15** (H-89), and **17** (HA-1004), which have IC_{50}'s of 0.38 µM – 3.0 µM, are isoquinolines. Compounds **10** and **15** are well known in the literature for their PKA activity [51-53]. As evident in the X-ray structures of **12, 11** and **15** in complex with PKA [52], these compounds are ATP competitive. Compound **14** has an IC_{50} of 1 µM in the RSK2 assay and has previously been investigated as a CDK inhibitor [54]. The binding mode of **14** in the ATP site of PAK4 (PDB code 2CDZ) has been determined in the crystal.

Compound **19** is the weakest RSK2 inhibitor presented in this paper; however, it is reported to be an ATP-competitive and selective inhibitor of c-JNKs, possessing a Ki of 0.19 µM [55]. The determination of the X-ray structure of **19** in complex with c-JNK (PDB code 1UKI) [56] confirms the binding of **19** at the ATP site.

In conclusion, our energy refined, all-atom binding models of a chemically diverse set of RSK2 inhibitors highlight key protein-ligand atomic contacts of known RSK2 inhibitors, in addition to leads that lack specific structural details characterizing their RSK2 binding. Of particular note are the binding modes of the S-isomer of **2** and (B) **6** which delineate a stereochemical preference to binding. Furthermore, in addition to forming the typical hydrogen bonding pattern

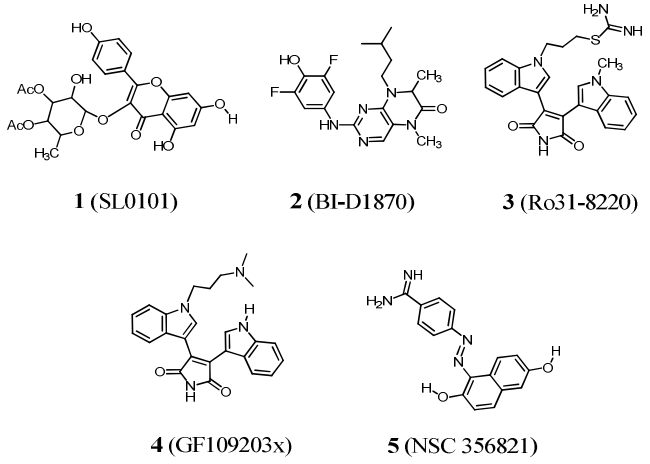

1 (SL0101) **2** (BI-D1870) **3** (Ro31-8220)

4 (GF109203x) **5** (NSC 356821)

Figure 1. Chemical structures of RSK2 inhibitors already reported in the literature.

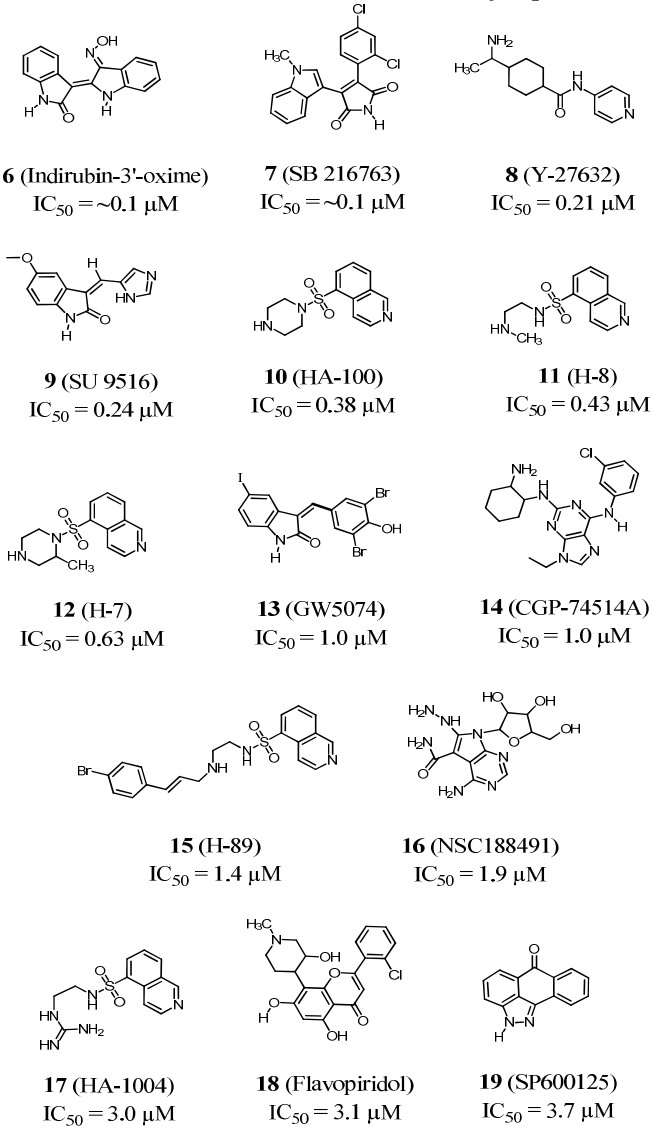

6 (Indirubin-3'-oxime)
IC_{50} = ~0.1 μM

7 (SB 216763)
IC_{50} = ~0.1 μM

8 (Y-27632)
IC_{50} = 0.21 μM

9 (SU 9516)
IC_{50} = 0.24 μM

10 (HA-100)
IC_{50} = 0.38 μM

11 (H-8)
IC_{50} = 0.43 μM

12 (H-7)
IC_{50} = 0.63 μM

13 (GW5074)
IC_{50} = 1.0 μM

14 (CGP-74514A)
IC_{50} = 1.0 μM

15 (H-89)
IC_{50} = 1.4 μM

16 (NSC188491)
IC_{50} = 1.9 μM

17 (HA-1004)
IC_{50} = 3.0 μM

18 (Flavopiridol)
IC_{50} = 3.1 μM

19 (SP600125)
IC_{50} = 3.7 μM

Figure 2. Chemical structures and inhibitory activities of RSK2 inhibitors used in this study.

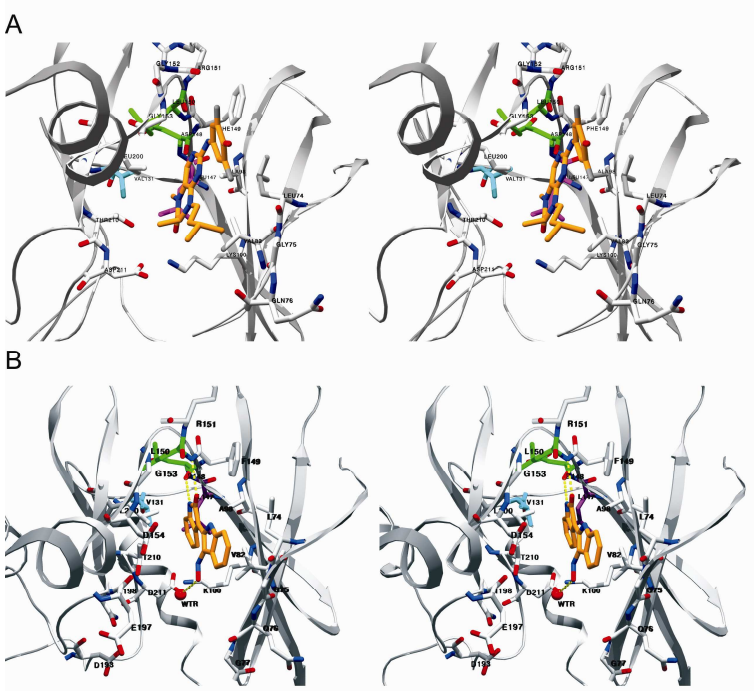

Figure 3. Stereoviews of the binding models of (A) S-isomer of 2 and (B) 6.

RSK2 is rendered in grey ribbon. The inhibitors and binding site residues are shown in stick. Nitrogen, oxygen and halogen atoms are colored blue, red, and purple, respectively. The carbon atoms are colored orange for the inhibitors, green for Asp148 and Leu150, which highlights the interior of the ATP-binding site, and cyan for Val131 and purple for Leu147, which demark key hydrophobic interaction sites. For clarity, hydrogen atoms are not depicted.

at ATP sites, compounds exhibiting inhibitory properties usually interact with side chain components of Asp148 and Leu150, which encompass a deeper interior component of the RSK2 ATP-binding site, and of particular interest from this study, ligands that form key hydrophobic contacts with Val131 and Leu147, are common to the most potent RSK2 inhibitors.

Acknowledgment

The research described herein was sponsored by the U.S. Army Medical Research and Material Command Research Plan #02-4-3U-057 and IAA #Y3-CM-100505 (MRMC and NCI). This project has been funded in whole or in part with federal funds from the National Cancer Institute, National Institutes of Health, under contract N01-CO-12400. The content of this publication does not necessarily reflect the views or policies of the Department of Health and Human Services, nor does mention of trade names, commercial products, or organizations imply endorsement by the U.S. Government. This research was supported in part by the Developmental Therapeutics Program in the Division of Cancer Treatment and Diagnosis of the National Cancer Institute. We acknowledge the National Cancer Institute for providing the compounds and for the allocation of computing time and staff support at the Developmental Therapeutics Program Computing Center and the Advanced Biomedical Computing Center.

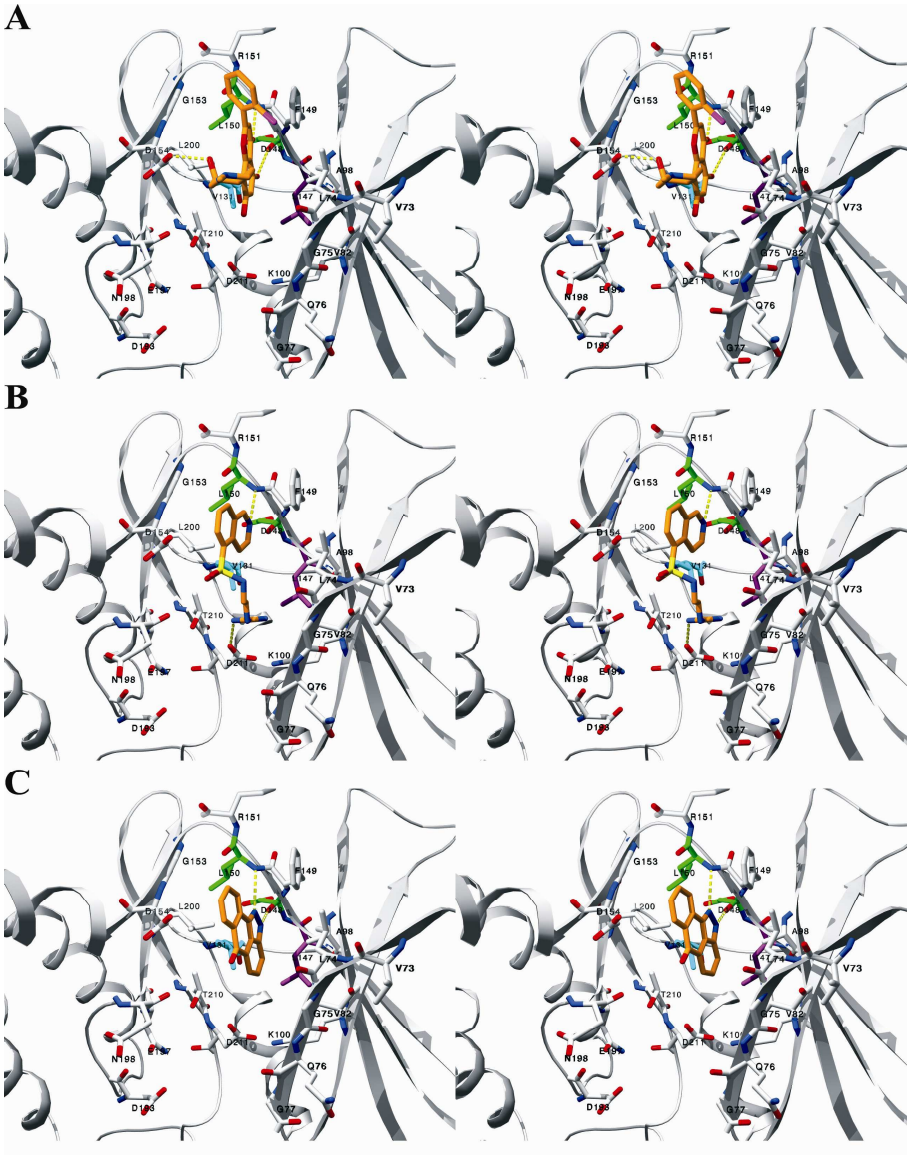

Figure 4. Stereo view of the binding models of the lower affinity inhibitors (A) 16, (B) 17, and (C) 18 rendered in the same fashion as in Figure 3.

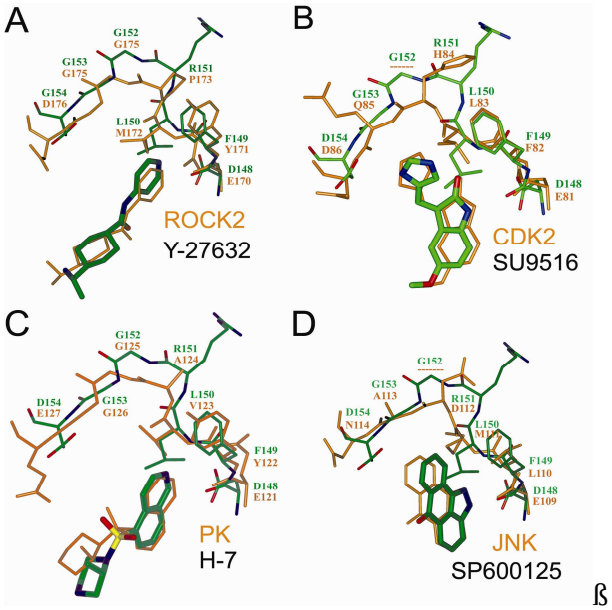

Figure 5. Comparison of the RSK2 binding models of 8, 9, 12, and 19 with their counterpart X-ray structures in other serine/threonine kinases.

*The ligands and residues are rendered in stick. The atoms of CDK2, ROCK2, PKA, and c-JNK and their bound ligands are colored orange, while nitrogen, oxygen and carbon atoms of RSK2 and its bound ligands are colored blue, red, and green, respectively. The residue names and numberings are colored green for RSK2 and orange for CDK2, ROCK2, PK, and c-JNK. (A) Compound **8** in PKA (PDB code 1YDR). (B) Compound **9** in CDK2 (PDB code 1PF8). (C) Compound **12** in ROCK2 (PDB code 2H9V). (D) Compound **19** in c-JNK (PDB code 1UKI).*

Table 1. The contact patterns of high affinity ligands 2 and 6 and lower affinity ligands 17, 18, and 19 with RSK2 based on the binding models.

The residue-ligand contacts were based on atom-atom distances of less than 4.5 Å and involved more than a single type of hydrogen-hydrogen contact. Val131 (colored cyan) and Leu147 (colored purple) are common to the most potent inhibitors but not the weaker binders.

	Residues within 4.5 Å of inhibitor
#	74 82 98 100 131 147 150 154 193 197 200 210 | | | | | | | | | | | | LGQGSFGKV AMK V LDFLRGGD DLKPENIL TD
2	LGQ V A K V LDFLRGG L TD
6	LG V A K V LDFL L TD
17	LG V K DFL GD L TD
18	L A DFLR GD L
19	A DFL GD L

REFERENCES

[1] SW Jones; E Erikson; J Blenis; JL Maller; RL Erikson. *Proc Natl Acad Sci U S A*, **1988**, 85 (10), 3377-81.
[2] DA Alcorta; CM Crews; LJ Sweet; L Bankston; SW Jones; RL Erikson. *Mol Cell Biol*, **1989**, 9 (9), 3850-9.
[3] DE Moller; CH Xia; W Tang; AX Zhu; M Jakubowski. *Am J Physiol*, **1994**, 266 (2 Pt 1), C351-9.
[4] Y Zhao; C Bjorbaek; S Weremowicz; CC Morton; DE Moller. *Mol Cell Biol*, **1995**, 15 (8), 4353-63.
[5] TL Nguyen. *Anticancer Agents Med Chem*, **2008**, 8 (7), 710-6.
[6] R Anjum; J Blenis. *Nat Rev Mol Cell Biol*, **2008**, 9 (10), 747-58.
[7] JP Delaunoy; A Dubos; P Marques Pereira; A Hanauer. *Clin Genet*, **2006**, 70 (2), 161-6.
[8] P Marques Pereira; A Schneider; S Pannetier; D Heron; A Hanauer. *Eur J Hum Genet*, **2009**,
[9] C Hetzer; D Bisgrove; MS Cohen; A Pedal; K Kaehlcke, et al. *PLoS ONE*, **2007**, 2, e151.
[10] DE Clark; TM Errington; JA Smith; HF Frierson, Jr.; MJ Weber; DA Lannigan. *Cancer Res*, **2005**, 65 (8), 3108-16.
[11] YY Cho; K Yao; A Pugliese; ML Malakhova; AM Bode; Z Dong. *Cancer Res*, **2009**, 69 (10), 4398-406.
[12] S Kang; S Elf; K Lythgoe; T Hitosugi; J Taunton, et al. *Journal of Clinical Investigation*, **2010**, 120 (4), 1165-77.
[13] M Buck; M Chojkier. *PLoS One*, **2007**, 2 (12), e1372.
[14] W Xian; L Pappas; D Pandya; LM Selfors; PW Derksen, et al. *Cancer Res*, **2009**, 69 (6), 2244-51.
[15] S Kang; S Dong; TL Gu; A Guo; MS Cohen, et al. *Cancer Cell*, **2007**, 12 (3), 201-14.
[16] TA Vik; JW Ryder. *Biochem Biophys Res Commun*, **1997**, 235 (2), 398-402.
[17] IA Leighton; KN Dalby; FB Caudwell; PT Cohen; P Cohen. *FEBS Lett*, **1995**, 375 (3), 289-93.
[18] M Malakhova; V Tereshko; SY Lee; K Yao; YY Cho, et al. *Nat Struct Mol Biol*, **2008**, 15 (1), 112-3.
[19] M Ikuta; M Kornienko; N Byrne; JC Reid; S Mizuarai, et al. *Protein Sci*, **2007**, 16 (12), 2626-35.
[20] M Malakhova; I Kurinov; K Liu; D Zheng; I D'Angelo, et al. *PLoS One*, **2009**, 4 (11),
[21] DJ Maloney; SM Hecht. *Org Lett*, **2005**, 7 (6), 1097-9.
[22] JA Smith; CE Poteet-Smith; Y Xu; TM Errington; SM Hecht; DA Lannigan. *Cancer Res*, **2005**, 65 (3), 1027-34.
[23] GP Sapkota; L Cummings; FS Newell; C Armstrong; J Bain, et al. *Biochem J*, **2007**, 401 (1), 29-38.
[24] A Morreale; B Mallon; G Beale; J Watson; M Rumsby. *FEBS Lett*, **1997**, 417 (1), 38-42.
[25] DR Alessi. *FEBS Lett*, **1997**, 402 (2-3), 121-3.
[26] TL Nguyen; R Gussio; JA Smith; DA Lannigan; SM Hecht, et al. *Bioorg Med Chem*, **2006**,
[27] J Bain; L Plater; M Elliott; N Shpiro; CJ Hastie, et al. *Biochem J*, **2007**, 408 (3), 297-315.
[28] P Bamborough; D Drewry; G Harper; GK Smith; K Schneider. *J Med Chem*, **2008**, 51 (24), 7898-914.
[29] DE Clark; CE Poteet-Smith; JA Smith; DA Lannigan. *Embo J*, **2001**, 20 (13), 3484-94.

[30] GE Kellogg; SF Semus; DJ Abraham. *J Comput Aided Mol Des*, **1991**, 5 (6), 545-52.
[31] RA Laskowski; JA Rullmannn; MW MacArthur; R Kaptein; JM Thornton. *J Biomol NMR*, **1996**, 8 (4), 477-86.
[32] T Clackson; JA Wells. *Science*, **1995**, 267 (5196), 383-6.
[33] I Collins; MD Garrett. *Curr Opin Pharmacol*, **2005**, 5 (4), 366-73.
[34] PC Chin; L Liu; BE Morrison; A Siddiq; RR Ratan, et al. *J Neurochem*, **2004**, 90 (3), 595-608.
[35] A Martinez; A Castro; I Dorronsoro; M Alonso. *Med Res Rev*, **2002**, 22 (4), 373-84.
[36] K Riento; AJ Ridley. *Nat Rev Mol Cell Biol*, **2003**, 4 (6), 446-56.
[37] Y Mukai; H Shimokawa; T Matoba; T Kandabashi; S Satoh, et al. *Faseb J*, **2001**, 15 (6), 1062-4.
[38] H Shimokawa. *J Cardiovasc Pharmacol*, **2002**, 39 (3), 319-27.
[39] S Ohki; K Iizuka; S Ishikawa; M Kano; K Dobashi, et al. *J Heart Lung Transplant*, **2001**, 20 (9), 956-63.
[40] AM Manning; RJ Davis. *Nat Rev Drug Discov*, **2003**, 2 (7), 554-65.
[41] G Manning; DB Whyte; R Martinez; T Hunter; S Sudarsanam. *Science*, **2002**, 298 (5600), 1912-34.
[42] M Mapelli; L Massimiliano; C Crovace; MA Seeliger; LH Tsai, et al. *J Med Chem*, **2005**, 48 (3), 671-9.
[43] JA Bertrand; S Thieffine; A Vulpetti; C Cristiani; B Valsasina, et al. *J Mol Biol*, **2003**, 333 (2), 393-407.
[44] ME Lane; B Yu; A Rice; KE Lipson; C Liang, et al. *Cancer Res*, **2001**, 61 (16), 6170-7.
[45] DJ Moshinsky; CR Bellamacina; DC Boisvert; P Huang; T Hui, et al. *Biochem Biophys Res Commun*, **2003**, 310 (3), 1026-31.
[46] X Yue; EV Varga; D Stropova; TW Vanderah; HI Yamamura; WR Roeske. *Eur J Pharmacol*, **2006**, 540 (1-3), 57-9.
[47] L Dugo; M Abdelrahman; O Murch; E Mazzon; S Cuzzocrea; C Thiemermann. *Shock*, **2006**, 25 (5), 485-91.
[48] H Yamaguchi; Y Miwa; M Kasa; K Kitano; M Amano, et al. *J Biochem (Tokyo)*, **2006**, 140 (3), 305-11.
[49] SP Davies; H Reddy; M Caivano; P Cohen. *Biochem J*, **2000**, 351 (Pt 1), 95-105.
[50] C Breitenlechner; M Gassel; H Hidaka; V Kinzel; R Huber, et al. *Structure*, **2003**, 11 (12), 1595-607.
[51] M Hagiwara; M Inagaki; M Watanabe; M Ito; K Onoda, et al. *Mol Pharmacol*, **1987**, 32 (1), 7-12.
[52] RA Engh; A Girod; V Kinzel; R Huber; D Bossemeyer. *J Biol Chem*, **1996**, 271 (42), 26157-64.
[53] A Zimmermann; H Keller. *Anticancer Res*, **1993**, 13 (2), 347-54.
[54] Y Dai; P Dent; S Grant. *Cell Cycle*, **2002**, 1 (2), 143-52.
[55] BL Bennett; DT Sasaki; BW Murray; EC O'Leary; ST Sakata, et al. *Proc Natl Acad Sci U S A*, **2001**, 98 (24), 13681-6.
[56] YS Heo; SK Kim; CI Seo; YK Kim; BJ Sung, et al. *Embo J*, **2004**, 23 (11), 2185-95.